Chemical Papers (2022) 76:1019–1030
https://doi.org/10.1007/s11696-021-01911-5

ORIGINAL PAPER

First characterization of functionalized nanoparticles—tandem of biosynthesized silver nanoparticles conjugated with piperine

Katarina Smilkov[1] · Darinka Gjorgieva Ackova[1] · Aleksandar Cvetkovski[1] · Nikola Geskovski[2] · Biljana Pejova[3] · Blazo Boev[4] · Petre Makreski[3]

Received: 26 June 2021 / Accepted: 27 September 2021 / Published online: 15 October 2021

Abstract

The present work outlines the biosynthesis of silver nanoparticles (AgNPs) using black pepper fruit extract (piperine) as bioreductive and capping agent, followed by their conjugation with piperine and characterization thereof. Several approaches for elucidation of the properites of both non-conjugated and piperine-conjugated AgNPs were implemented. The formation of silver nanoparticles was monitored at 420 nm, corresponding to the surface plasmon resonance band of the obtained AgNPs. SEM and AFM analyses demonstrated the spherical shape of the NPs, while the DLS analysis revealed the negative charge of the NPs with mean diameter of 116.6 ± 8.9 nm and 142.1 ± 10.7 nm for AgNPs and piperine-conjugated AgNPs, respectively. Characteristic Raman bands at 237 cm^{-1} for AgNPs and at 249 cm^{-1} for piperine-AgNPs, indicate Ag^{+} reduction to nanoscaled Ag, in addition to emergence of new bands as a result of the formation of bonds with oxygen atoms from the extracted organic molecules. The bands in the Amide I region characteristic for β-sheets in the structure, followed by bands from the α-helices were also assigned. The work represents the first conjugation of the AgNPs with bioactive piperine, that further might be evaluated as promising new delivery system in the pharmaceutical and biomedical industry.

Graphical abstract

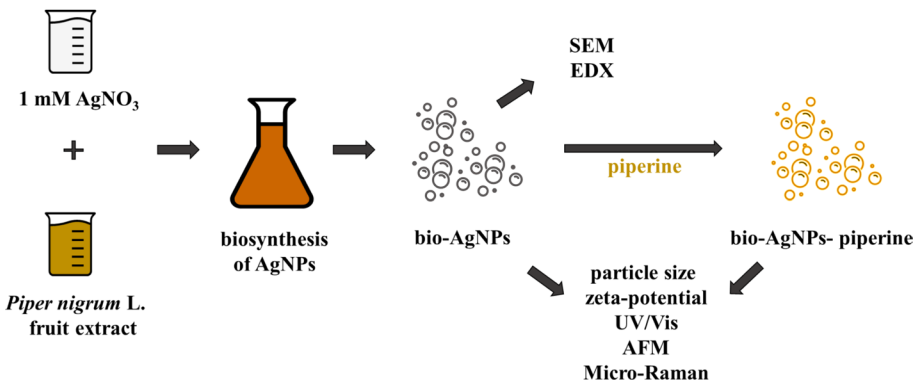

Keywords Biosynthesized nanoparticles · Silver nanoparticles · Piperine · Plant bioactive

Introduction

The formulation of bioactive nanoparticles (NPs) demands interdisciplinary efforts of chemical, biomedical, and pharmaceutical research. Recently, the focus was sharpened to fabricate functionalized NPs with improved antioxidant/antimicrobial properties (Sanpui et al. 2011; Reddy et al.

Katarina Smilkov and Darinka Gjorgieva Ackova contributed equally to this work.

✉ Katarina Smilkov
katarina.smilkov@ugd.edu.mk

Extended author information available on the last page of the article

2014; Abdel-Rahman et al. 2016; Gour and Jain 2019; Abu-Dief et al. 2020). Various approaches stem for the synthesis of NPs including physicochemical methods, as ultrasound, UV radiation or photochemical reduction (Sau et al. 2001; Okitsu et al. 2001; Sun 2013), though the use of toxic agents in some of these methods are potentially dangerous both to humans and the environment (Montes-García et al. 2014; Shaik et al. 2018). Therefore, substituting hazardous and toxic solvents, stabilizers, and reducing agents with water soluble natural compounds favored green chemistry synthesis of inorganic NPs (Saddik et al, 2021). Among the available methods for biosynthesis, the fabrication of NPs using plant extracts provide an important alternative toward the functionalization of the materials (Adil et al. 2015; Rauf et al. 2021). The reduction capacity of natural plant extracts arises directly from the various compounds that contain $–NH_2$, –COOH, –OH, –SH, and other functional groups, most broadly classified as functional groups included in the molecular structure of polyphenols (Obaid et al. 2017; Shaik et al. 2018). These plant biomolecules possess a strong reducing ability and tendency for surface adsorption, which can functionalize the obtained NPs and provide them with new properties (Khan et al. 2013; Li et al. 2013). Biosynthesized NPs are claimed to be more biocompatible and can be applied without any further modifications (Mie et al. 2014).

The antibacterial properties of silver and, moreover, silver NPs (AgNPs) have been widely studied (Medjhouda Kebir et al. 2018; Abdelkrim et al. 2020; Azmi et al. 2021). However, the "hidden" potential of functionalized NPs has not been explored, especially their anticancer, antiviral, antifungal, and even antioxidant properties (Zhang et al. 2016; Rauf et al. 2021).

Despite the known physicochemical and biological characterization mentioned above, more detailed information about the physical, chemical, and optical properties of the nanoparticles still remains scarce. Here, we climb a step further by performing a joint spectroscopic-microscopic-optical investigation of biosynthesized and functionalized silver nanoparticles.

In the current study, we have used piperine—the bioactive compound of black pepper (*Piper nigrum* L.) (Gorgani et al., 2017) as an agent for both bioreductive and capping properties for the biosynthesis of AgNPs. Black pepper is rich in various secondary plant metabolites, as alkaloids, flavonoids, and terpenoids, which contribute greatly to its reducing capability. Moreover, the most abundant alkaloid, piperine (1-(5-[1,3-benzodioxol-5-yl]-1-oxo-2,4-pentadienyl) piperidine) is recognized for its antioxidant and anticancer properties (Reddy et al. 2014; Smilkov et al. 2019; Alves et al. 2020).

The previous findings initiated and postulated the aim of the work in the following consecutive sections: biogenic synthesis of AgNPs using the extract of this plant, further conjugated with piperine, and their characterization using different complementary methodologies: UV/Vis spectrophotometry, Dynamic Light Scattering (DLS), Scanning Electron Microscopy (SEM), Atomic Force Microscopy (AFM), Energy Dispersive X-ray (EDX), and Raman spectroscopy.

Experimental

Materials

Chemicals

Food-grade *Piper nigrum* fruit was purchased from the local market, whereas piperine (98%) was purchased from Acros Organics, Belgium. Silver nitrate, RPE, and ACS (Carlo Erba Reagents, Italy) were selected as a silver precursor. The 96% ethanol (Ph.Eur, Carlo Erba Reagents, Italy) was used for dissolving piperine.

Methods

Preparation of the aqueous extract from Piper nigrum fruit

2.5 g of dried and fine-grinded *Piper nigrum* fruit powder was added to 100 mL deionized ultrapure water in 250 mL Erlenmeyer flask. The preparation of aqueous *Piper nigrum* fruit extract was done by using heating stirrer at 100 °C for 20 min in reflux extraction. The extract was filtered through Whatman filter paper No.1.

Biosynthesis of silver nanoparticles by using plant capping agent

The biosynthesis of bio-AgNPs was carried out by adding 2.5 mL of *Piper nigrum* fruit aqueous extract to 47.5 mL of 1 mM silver nitrate solution, and the reaction mixture was kept at room temperature for 2 h. The overall incubation process was carried out at room temperature, using an orbital shaker (MRC) and in dark conditions to avoid possible photochemical reactions. A color change of the solution from colorless to brownish yellow was observed. The reduction in silver ions by plant extract occurred as the time elapsed whereas the formation of the silver nanoparticles was confirmed by UV/Vis spectroscopy. The obtained AgNPs (denoted bio-AgNPs in the forthcoming text) were purified through centrifugation at 6000 rpm for 20 min, washed with deionized water, and collected for characterization purposes.

Conjugation of piperine in biosynthesized AgNPs (bio-AgNPs-piperine)

The collected bio-AgNPs were suspended in water and treated by adding 1 mg/mL solution of piperine in ethanol. The mixture was sonicated for 30 min, and the resulting suspension (bio-AgNPs-piperine) was used for further characterization by Raman spectroscopy.

Characterization of bio-AgNPs and bio-AgNPs-piperine

Monitoring of AgNPs formation The progress of AgNPs formation was analyzed using BOECO S-300 (Germany) UV/Vis spectrophotometer at 420 nm. Briefly, the absorbance of the reaction sample was recorded every 5 min for five consecutive hours to determine the equilibrium of the reduction reaction and to optimize the incubation time. Full UV/Vis spectrum (200–800 nm) was recorded for each sample at the end of the preparation stage.

Determination of hydrodynamic diameter and zeta potential The mean hydrodynamic diameter (Dh) and zeta potential (ZP) were analyzed using dynamic light scattering apparatus Zetasizer Nano ZS (MalvernPanalytical, UK). The native samples (water dispersions) were transferred into a folded capillary cell, and the parameters (attenuator index, measurement position, duration and voltage) were automatically optimized for each size and zeta measurements. The samples were analyzed in triplicates.

Scanning Electron Microscopy (SEM) The morphology and spectral analysis of bio-AgNPs was determined by using Scanning Electron Microscope (SEM VEGA3 LMU and INCAEnergy 250 EDS X-ray Microanalysis System). The aqueous suspension of bio-AgNPs was loaded dropwise on a carbon-coated copper grid and left to dry for few minutes at room temperature before scanning.

Atomic Force Microscopy (AFM) AFM measurements were performed on a scanning probe microscope (SPM 9600 produced by Schimatzu Co.) using a dynamic and phase mode of operation. Bio-AgNPs deposits were prepared onto squared glass substrates (7 mm × 7 mm) following ex situ deposition protocol (*i.e.,* dropping few drops of AgNPs suspension onto a glass substrate and subsequent evaporation of liquid phase). The investigated samples were scanned at few points in 2 µm, 1 µm, and 500 nm scanning area with a scan rate of 1 Hz and resolution of 512 lines per scan direction. The frequency and force constant of the used AFM tip were 320 kHz and 42 N/m correspondingly. The obtained AFM microphotographs were processed and analyzed using the VectorScan software package. The recorded images were just flattened, and no additional processing was performed.

Micro-Raman spectroscopy Micro-Raman spectra were recorded using Horiba JobinYvon Labram 300 multichannel spectrometer in the 100–2000 cm^{-1} spectral range. The backscattered radiation (180° configuration) was analyzed with an 1800 lines/mm difraction grating. An Olympus MPlanN confocal microscope with a × 50 objective (NA 0.75) was selected. The pinhole aperture to regulate the confocality degree was fixed to 500 µm, while the entrance slit for control of the spectral resolution of the spectrometer was adjusted to 100 µm. The red He:Ne excitation laser with 632.8 nm was selected, at first, without applying a filter for laser power attenuation (4.21 mW; power density of 505.9 kW/cm^2). Due to the evident burning of the sample, the intensity of the laser was subsequently adjusted by adding attenuation filters (1.9 mW and power density of 228.3 kW/cm^2; 0.97 W; power density of 116.6 kW/cm^2; 0.46 mW; power density of 55.3 kW/cm^2) to that extent that no photoinduced burning of the sample was achieved. Raman intensities were collected with a thermo-electrically cooled CCD array detector. The resolution of the system was 3 cm^{-1} and the wavenumber accuracy, calibrated with the Rayleigh line and the 520.5 cm^{-1} line of a Si standard, was ± 1 cm^{-1}. The spectra were collected with 8 s acquisition period and × 5 averaging. Bright-field micrograph from each sample was taken at × 50 magnification after each scanning.

Results and discussion

UV/Vis spectrophotometry

Previous research showed that the amount of plant used, and the concentration of the extract set to perform the reduction of silver, influences the UV/Vis spectral features (Andalakshmi et al., 2016). Our study revealed the presence of a shoulder at 420 nm (Fig. 1A), that is assigned to surface plasmon resonance of the AgNPs smaller than 70 nm (Durán et al. 2011). Namely, various studies report the appearance of the surface plasmon resonance peak at wavelengths ranging from 410 to 450 nm, depending on the concentration and type of extract used (Jacob et al. 2012; Shaik et al. 2018). In further examination, we monitored the formation of the bio-AgNPs, during a period of 5 h, to determine the optimal incubation time for the bioreduction process. The study revealed that the concentration of the particles, in terms of the recorded absorbance at 420 nm, grows continuously. The increased absorbance as a function of time can be attributed to increased aggregation of the newly formed NPs, as previous research indicate that the size of the AgNPs largely contributes to the scattering effect that leads to an increase in the extinction coefficient (Paramelle et al., 2014). Therefore, the period of 2 h was set as incubation interval for the actual synthesis experiments (Fig. 1B).

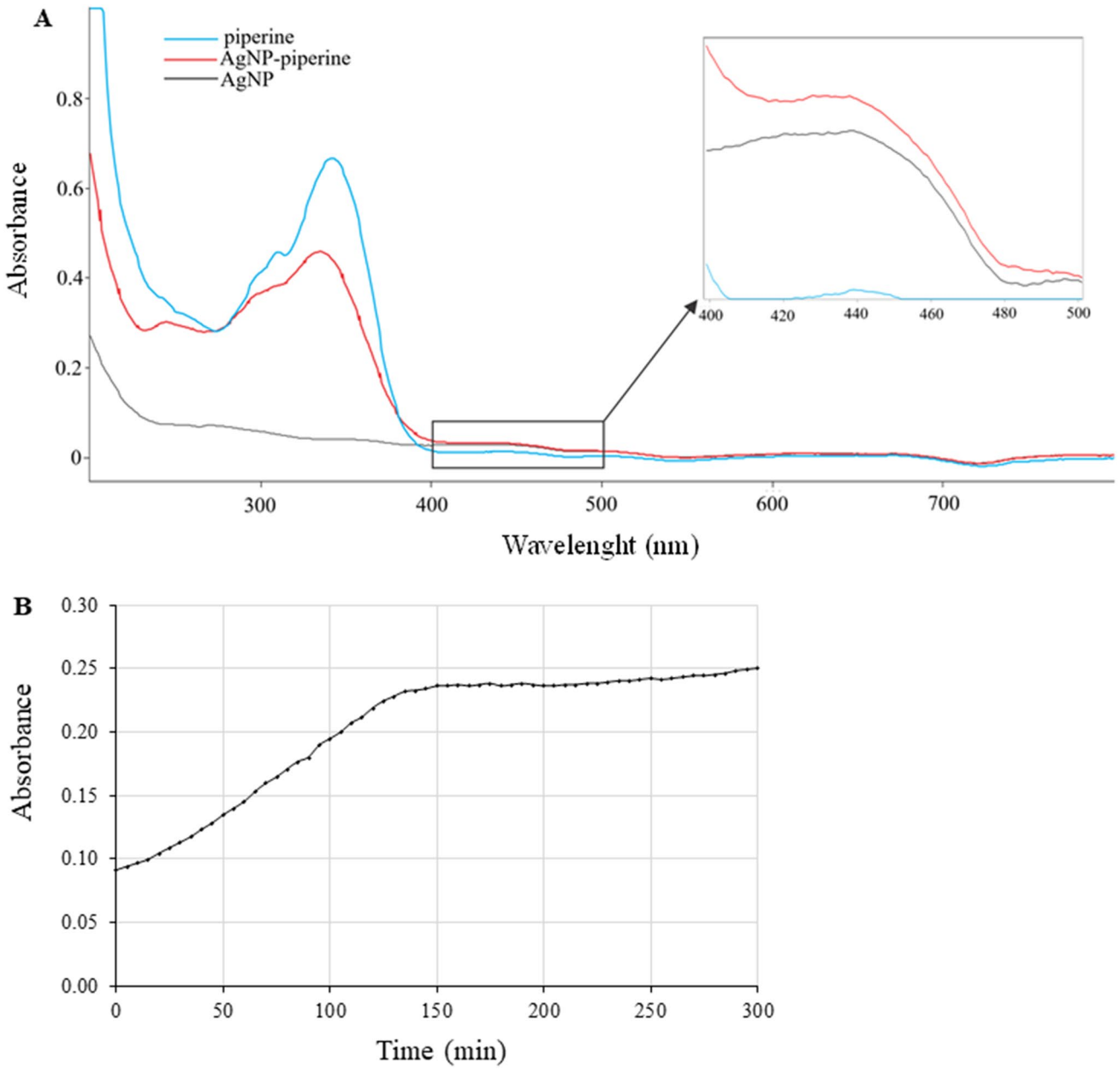

Fig. 1 (**A**) UV/Vis spectrum of bio-AgNP, bio-AgNP-piperine and piperine. The region of interest (400–500 nm) is enlarged (inset); (**B**) Plot of absorbance intensity at 420 nm at various time points during the synthesis of bio-AgNPs

Hydrodynamic diameter and zeta potential

The mean Dh of bio-AgNPs and bio-AgNPs-piperine was 116.6 ± 8.9 nm (PDI 0.611 ± 0.06) and 142.1 ± 10.7 nm (PDI 0.582 ± 0.05), while the ZP was -12.2 ± 1.23 mV and -3.03 ± 0.26 mV, respectively. The results indicate that both samples were in the nanometer range with monomodal distribution and rather large PDI (Fig. 2A), probably due to the conditions during the silver reduction (extract concentration, composition) that affect the nucleation and capping of the bio-AgNPs during the synthesis. The NPs are negatively charged and with the addition of piperine, the ZP approaches more neutral values (Fig. 2B), probably due to its adherence on the surface of bio-AgNPs. The piperine-induced changes in the surface of the AgNP are also evident by the rise of the Dh, which probably occurs due to the increase in the ZP to neutral values which allows more intimate NP contacts and further particle aggregation.

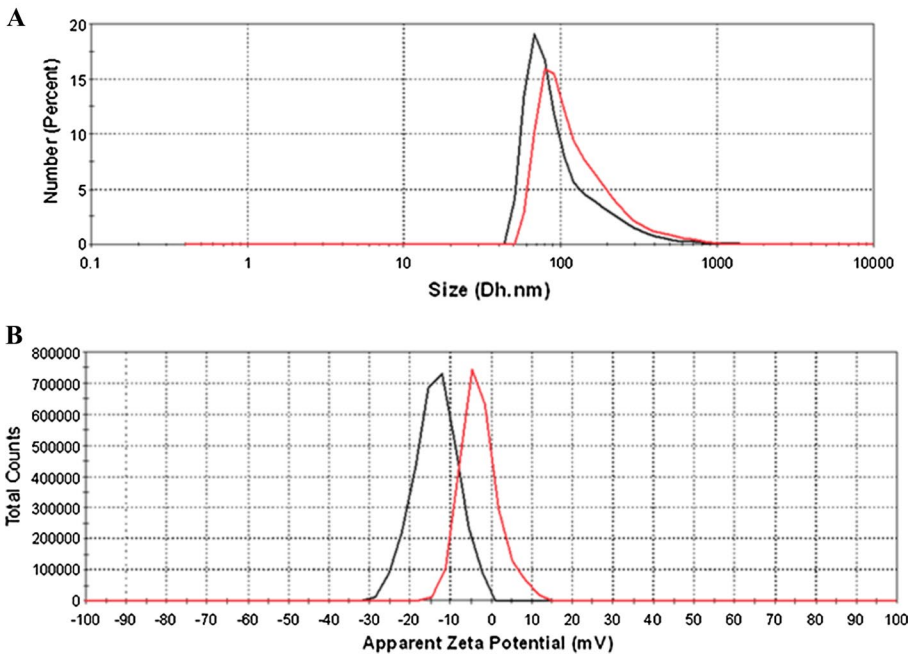

Fig. 2 (**A**) Particle size distribution and (**B**) Zeta potential of bio-AgNPs (black line) and bio-AgNPs-piperine (red line)

SEM and EDX analysis

SEM studies revealed the characteristics of the synthesized bio-AgNPs, which were additionally confirmed by AFM analysis. SEM analysis of the synthesized bio-AgNPs depicted the predominantly spherical shape of the particles with the size of around 65 nm, and an additional population of irregularly shaped particles, that demonstrate a tendency to form aggregates (Fig. 3). Our synthesis method resulted in a larger size of the obtained bio-AgNPs, relative to the similarly synthesized AgNPs reported by Jacob et al. (2012). On the other hand, the obtained size was found similar to the average size diameter of the AgNPs produced by fungi *Rhodotorula glutinis* and *R. mucilaginosa*, ranging from 56 to 85 nm (Agressott et al. 2020). Despite the morphology and degree of

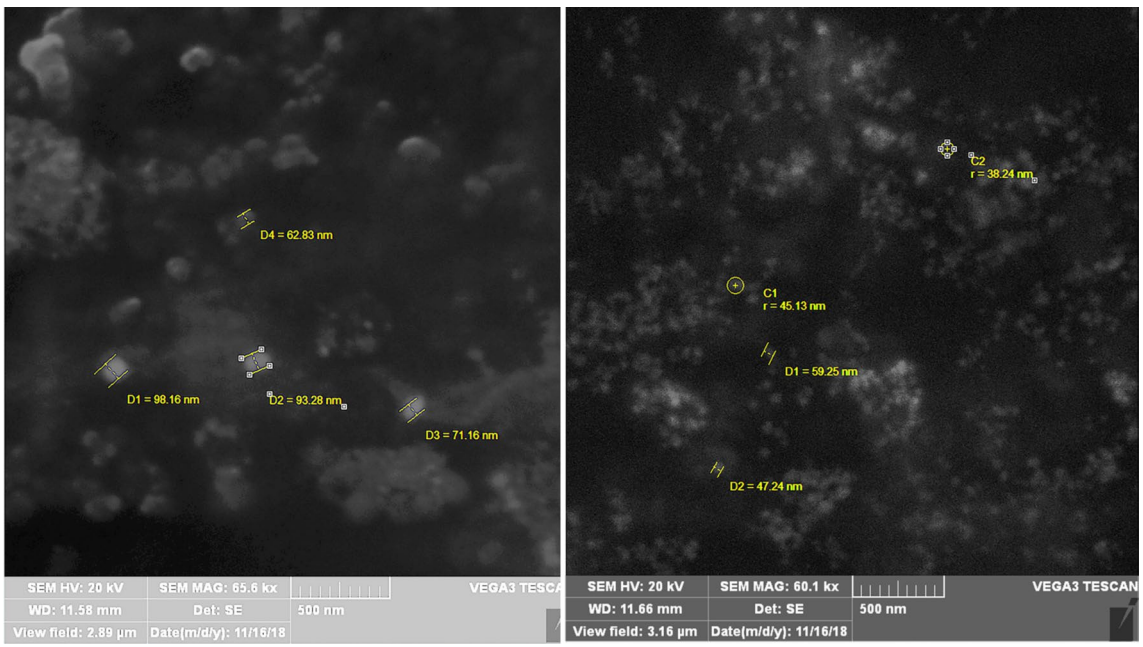

Fig. 3 SEM image in two different view fields, showing well-dispersed AgNPs formed by bioreduction method, and their corresponding size

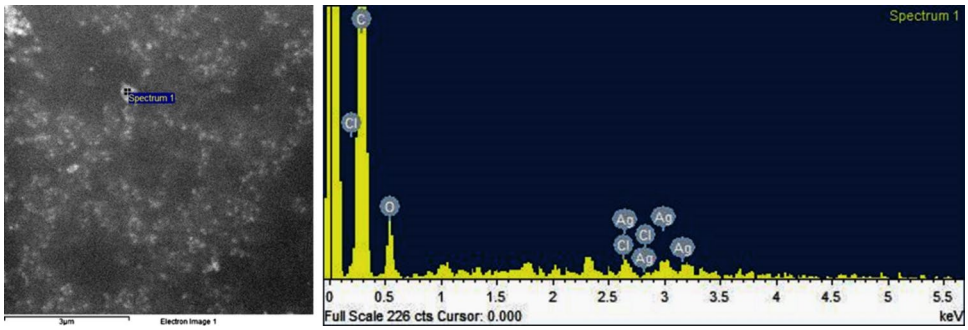

Fig. 4 SEM–EDX results of the fabricated nanoparticles: (**A**) SEM view of the selected field for analysis; (**B**) EDX spectrum presenting the elements detected in the selected field

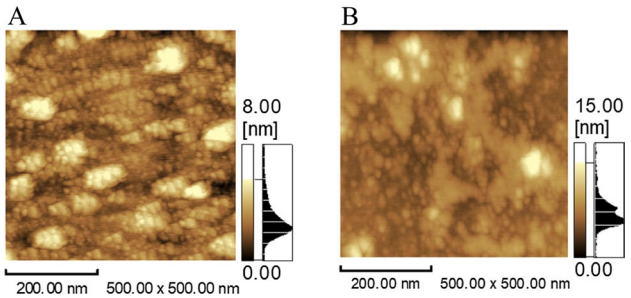

Fig. 5 2D AFM images of (**A**) bio-AgNPs and (**B**) bio-AgNPs-piperine deposits

particle aggregation evidenced by SEM (Fig. 4A), an EDX spectroscopy was undertaken, to elementally map the chemical composition of the nanoparticles. EDX spectrum shows relatively strong peaks from the presence of silver along with chlorine, oxygen, carbon, and sodium. The distinguishable intense peaks of Ag that appeared in the EDX spectrum at approximately 3 keV (Fig. 4B) confirmed the formation of Ag nanoparticles corresponding to the previously reported results (Mollick et al. 2015; Anandalakshmi and Venudobal 2017).

Atomic Force Microscopy results

AFM was performed to depict the nanosized dimensions of the formed bio-AgNPs and bio-AgNPs-piperine particles (Fig. 5). The results revealed no significant difference in nanoparticle size obtained by the two used experimental approaches (*i.e.,* with and without the presence of piperine). However, on the other hand, the used experimental conditions influenced the ordering of bio-AgNPs. It is obvious that bio-AgNPs are closely packed in comparison with bio-AgNPs-piperine where protein-capping layer structure seemed to be easily disturbed, which is an important sign of achieving plant bioactive conjugation (piperine).

Figures 6 and 7 show 3D-views of bio-AgNPs and bio-AgNPs-piperine deposit's surfaces. Apparently, no significant difference in the roughness of surfaces formed by both deposits was evidenced that nicely complements the calculated values for the average roughness (R_a) parameter (Table 1).

Raman spectroscopy

Raman spectroscopy was applied for extensive characterization of bio-AgNPs and bio-AgNPs-piperine samples by monitoring the bands occurring mainly from the structural amide group vibrations. To detect possible functional groups of the plant reducing agent involved in the formation and

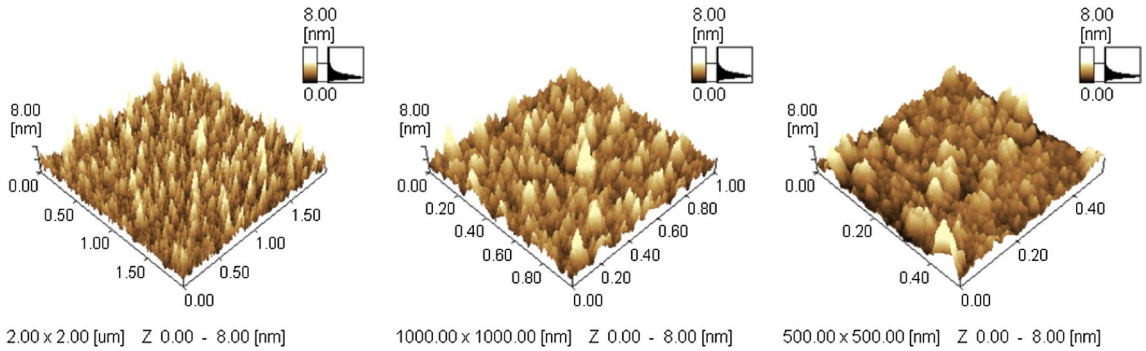

Fig. 6 3D AFM images of bio-AgNPs deposits

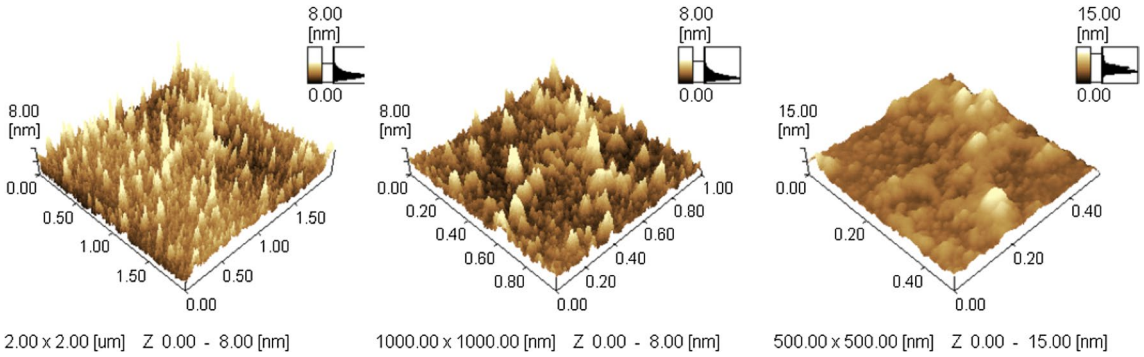

Fig. 7 3D AFM images of bio-AgNPs-piperine deposits

Table 1 Calculated values for average roughness (R_a) parameter

Sample	R_a/nm
Bio-AgNPs deposit	1.1024 ± 0.0607
Bio-AgNPs-piperine deposit	1.2868 ± 0.1503

stabilization of bio-AgNP, the acquired Raman spectrum (2000–200 cm^{-1}) (Fig. 8A) was subsequently compared to the first collected spectrum of bio-AgNPs-piperine where attenuation filter was also not used (Fig. 8B). The Raman spectrum of bio-AgNPs (Fig. 8A and B(a)) depicted the

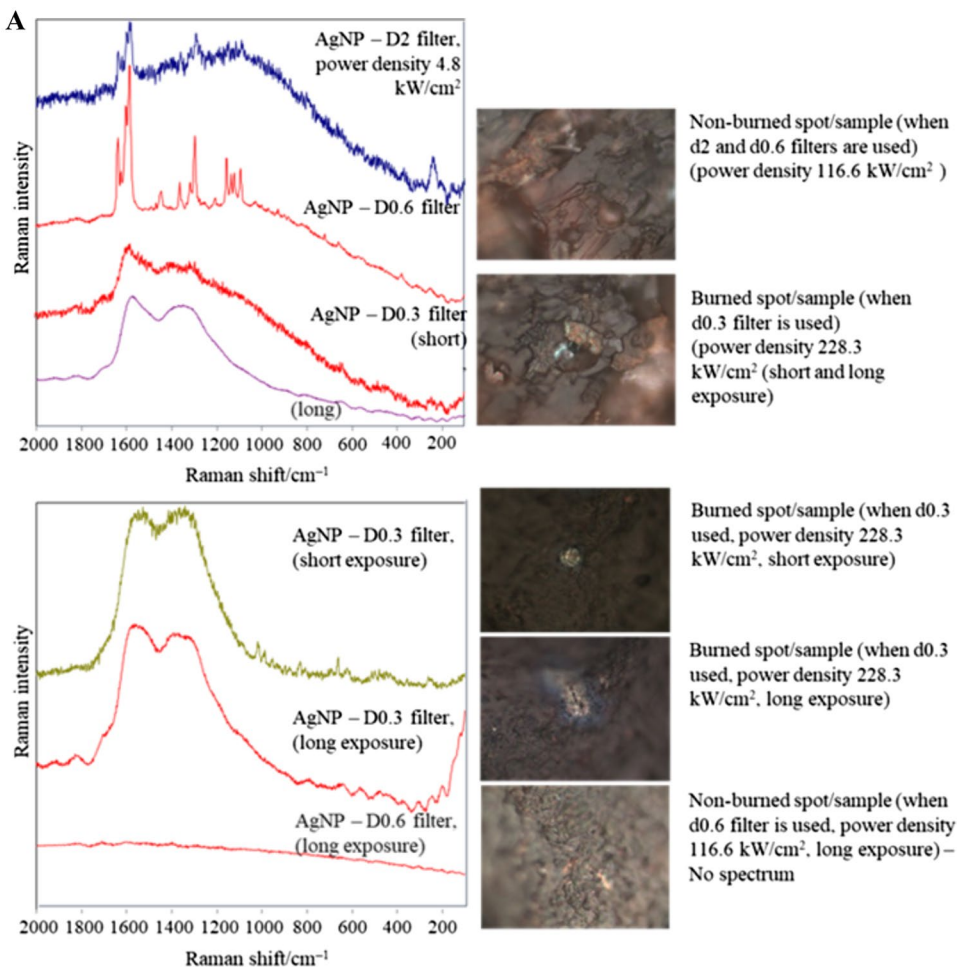

Fig. 8 Recorded Raman spectra of synthesized bio-AgNPs (**A**) and bio-AgNPs-piperine (**B**)

Fig. 8 (continued)

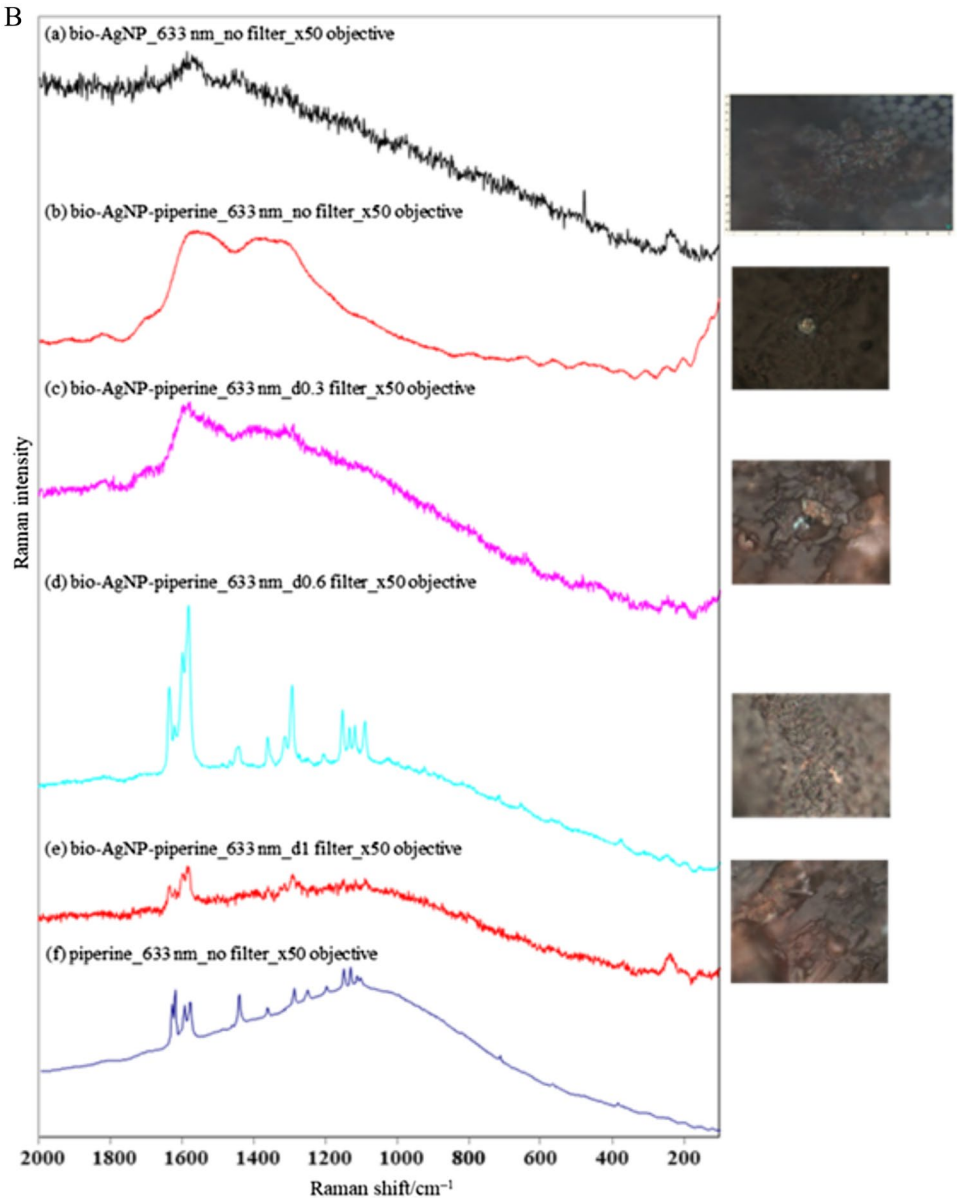

characteristic peak at 237 cm^{-1}, attributed to the Ag–O stretching vibrations indicating that: (i) Ag^{+} has been reduced to nanoscale Ag and (ii) oxygen atoms, present in the structure of some of the extracted organic molecules from the black pepper, are chemisorbed on the formed Ag nanoparticles. Despite this peak, the spectral signal-to-noise ratio is very weak and no other useful Raman peak could be evidenced except for the appearance of increased Raman signal around 1600 cm^{-1}. The stabilization of bio-AgNPs results from the capping plant bioactive structures, usually oligopeptides, that lie on the surface of the nanoparticle increase the stability and prevent the oxidation of Ag^{0} to Ag^{+} (Agressott et al. 2020).

In line with this observation, the initially recorded Raman spectrum of the bio-AgNP-piperine sample without attenuation of the laser intensity also depicted a rather peculiar signature (Fig. 8B(b)). The spectrum shows two complex, broad and, to some extent, superimposed peaks with the centroids peaking at 1563 and 1360 cm^{-1}. Such spectral view completely resembles the spectrum of carbon nanotubes (Dresselhaus et al. 2005) inferring that the present organic components have been carbonized (burned) due to the strong incident laser power. Such demonstration is confirmed by the optical micrograph taken after the spectrum was scanned (Fig. 8B(b)). A possible explanation for the instabilities noted in the Raman spectra might be related to different events as modifications of the Ag-core, e.g., detectable changes in its shape, heating, or melting due to the laser energy transfer.

This conclusion addressed the need to recollect the spectrum by lowering the laser intensity with the use of the attenuation filter (Fig. 8B(c)) which resulted in a practically unimproved scenario despite the better observation of the previously discussed Ag–O peak. Keeping the same experimental conditions, further decrease in the laser intensity caused better Raman spectrum where no carbonization took place evidenced by the appearance of well-defined and sharp peaks particularly pronounced in the 1700–1000 cm^{-1} region. In addition, the corresponding bright optical micrograph showed that no sample degradation occurred (Fig. 8B(d), right image). The tentative assignment of the vibrational bands is presented in Table 2.

The 249 cm^{-1} peak (Fig. 8B(d)) indicates the formation of Ag–O bonds (Biswas et al. 2007; Kora and Arunachalam 2012) which is even more pronounced in the spectrum collected by the strongest attenuation filter (Fig. 8B(e)). Thus, we can explain the formation and stabilization of bio-AgNP-piperine by chemical bonding of the oxygen atom (from the carbonyl group present in the piperine molecule) with the silver atom (Mukherjee et al. 2008). The C=O carbonyl group manifests evolution of the Raman peaks attributed to the amide I bands occurring at 1632 and 1620 cm^{-1}. Further, the strong bands at 1599 and 1583 cm^{-1} could be attributed to the asymmetric C=O stretching vibrations from the carboxylate group that might be formed in the redox reaction between the water dissolved sugars (part of the composition of the black pepper) and Ag^+ cation, leading to the formation of carboxylate group and AgNPs. The corresponding C = O symmetric carboxylate sugar vibrations gave rise to the Raman peaks registered at 1362 cm^{-1} (Fig. 8B(d)). The bands around 1465 and 1446 cm^{-1} could be tentatively prescribed to overlay the C–H bendings from the conjugated C–C chain in piperine (or from the aryl ring) with the asymmetric CH_2 bendings from the sugars (Lazarevska et al. 2019). Going toward lower wavenumbers, the strong bands at 1313 and 1294 cm^{-1} could be attributed to the C–N stretching vibration from the N–C = O moiety in piperine whose position nicely fit the amide III (NH and CH bendings) bands (Lazarevska et al. 2019; Alves et al. 2020). The C–C– (piperidine ring) stretch bands were observed in the range of 1158 and 1294 cm^{-1} in the spectra of bio-AgNPs-piperine, provides excellent correlation with Raman vibrational data for piperine alkaloid (Fig. 8B(f)). Our results are in concordance with previously studied Raman spectra of pure piperine crystals isolated from pepper, black pepper, and related oleoresin reported in the literature (Schulz et al. 2005; Alves et al. 2020).

The correlation between the band frequency and the secondary structure of the protein arises from the hydrogen bonding between the polypeptide bonds being different in α-helix, β-sheet, or disordered structures (Rygula et al., 2013). The used plant extract, as a bioreductive and capping agent for the biosynthesis of AgNPs, is rich with different plant metabolites (sugars, proteins, alkaloids, flavonoids, terpenoids). Among them, oligopeptides, that are present on the surface of the nanoparticles are involved in their stabilization in a way that prevents the oxidation of Ag^0 to Ag^+ (Agressott et al., 2020).

A strong band in the region between 1612 and 1640 cm^{-1} and a weaker band around 1685 cm^{-1} are commonly observed for β-sheets in the structure associated by weak bands at lower frequencies (1665–1670 cm^{-1}). In proteins known to adopt α-helical conformation, strong amide I bands between 1650 and 1655 cm^{-1} emerged (Pelton and McLean, 2000). The appearance of a singlet Raman band around 1670 cm^{-1} is explained by the fact that amide I band of turns overlaps and overlays those of α-helices and β-sheets making its assignment difficult. The presence of unordered or random structure (α/β, α + β) in the samples corresponds to Raman blue-shifted band to 1665 cm^{-1}. The bands appearing at higher frequencies are attributed to the

Table 2 Assignments of the Raman bands (cm^{-1}) characteristic for bio-AgNPs and bio-AgNPs-piperine

Assignments (range in cm^{-1})	Bio-AgNPs	Bio-AgNPs-piperine
Amide VII (200–300)	237 s; 244sh; 365w	249 s
S–S; Tyr; Trp; N-Cα-C; C-S-C; (400–1000)	432; 512; 590w; 603sh; 690; 774; 875 s; 881sh; 962 m; 979sh; 989sh	395w; 577w; 658w; 727w; 822w; 876w; 931w;
Phe (1000–1100)	1096vw	1031w; 1099 s;
C-N (1100–1200)	1109w; 1123w; 1170vw	1122 s; 1140 s; 1158vs; 1167sh;
Amide III (CN stretching, NH bending) (1229–1301)	1267vw	1212w; 1294vs; 1313sh;
Trp, Cα-H (def) (1300–1400)	1341 s; 1388; 1448w; 1455sh;	1362 s; 1371sh; 1443w;
Amide II (CN stretching, NH bending—Indole ring-Trp; Tyr, Trp, Phe) (1480–1600)	1579vs; 1593sh	1583vs; 1599 s; 1616sh;
Amide I (C = O stretching/hydrogen bonding coupled with COO) (1660–1690)	1673w; 1700w; 1706; 1716	1620w; 1632sh; 1644 s; 1648sh

*v—very, w—weak, m—medium, s—strong, sh—shoulder

α-helix vibrations in the structure. Based on the band frequencies obtained for Amide I, II, and III bands, we predominantly registered bands in the Amide I region characteristic for β-sheet (antiparallel and parallel), followed by α-helices (Table 2, Fig. 8 (A and B)) (1673, 1700, and 1706 cm^{-1} for bio-AgNP and 1620, 1632, and 1644 cm^{-1} for bio-AgNP-piperine). Due to the large number of Raman peaks distributed in a wide range of frequencies, it is not possible to fully classify the present protein components according to their secondary structures (α-helix, β- sheet, and protein mixed structures) that rests in accordance with a previously published study by Agressott et al. 2020.

Conclusions

This research presents a fast, low-cost, simple, and effective method for biosynthesis of AgNPs by reducing the precursor silver nitrate with an aqueous extract of *Piper nigrum* fruit. The obtained NPs were predominantly spherical with a mean diameter of 116.6 nm and a negative surface charge. The abundance and availability of the black pepper makes this green method feasible for the large-scale production of bio-AgNPs.

Synthesis, characterization, and possible bio-applications of AgNPs, with special emphasis on antibacterial and anticancer activity, in both academic and industrial research are explored a lot recently. Although various methods are available, the synergistic effects of AgNPs and multiple therapeutic/nutraceutical agents (with anticancer activity, antibacterial effect or anti-inflammatory or antioxidant properties) were still obscure. Therefore, we synthesized and functionalized bio-AgNPs with piperine on their surface, which provides added value to the already known antioxidant and anticancer properties of AgNPs.

The change in the surface potential and the obtained Raman fingerprints of this new functionalized nanoparticles reveal a successful conjugation of bio-AgNPs with piperine. This result gives another perspective of the potential uses of this novel biosynthesized bio-AgNPs-piperine. The functionalized NPs can be regarded as interesting finding relevant for further examination in the field of targeted drug delivery and in vivo interactions.

Acknowledgements The authors acknowledge M.Sc. Maja Lazarova, from the Laboratory for Electronic Microscopy, University Goce Delčev-Štip, for the kind help with SEM analysis of the samples.

Author contributions All authors were involved in study conception and design. Katarina Smilkov and Darinka Gjorgieva Ackova performed the synthesis experiments, interpreted the results, and drafted the manuscript. Aleksandar Cvetkovski, Nikola Geskovski, Biljana Pejova, and Petre Makreski performed the analysis, acquired the data, and interpreted the results. Blazo Boev and Petre Makreski critically revised the manuscript. All authors have read, commented, and approved the final manuscript.

Funding No funding was received to assist with the preparation of this manuscript.

Declarations

Conflicts of interest The authors declare that they have no conflict of interest.

Data Availability All data generated or analyzed during this study are included in this published article.

References

Abdelkrim S, Mokhtar A, Djelad A, Bennabi F, Souna A, Benguedach A, Sassi M (2020) Chitosan/Ag-Bentonite Nanocomposites: Preparation, characterization, swelling and biological properties. J Inorg Organomet Polym 30:831–840. https://doi.org/10.1007/s10904-019-01219-8

Abdel-Rahman LH, Abu-Dief AM, El-Khatib RM, Abdel-Fatah SM (2016) Some new nano-sized Fe (II), Cd (II) and Zn (II) Schiff base complexes as precursor for metal oxides: Sonochemical synthesis, characterization, DNA interaction, in vitro antimicrobial and anticancer activities. Bioorg Chem 69:140–152. https://doi.org/10.1016/j.bioorg.2016.10.009

Abu-Dief AM, Abdel-Rahman LH, Abd-El Sayed MA, Zikry MM, Nafady A (2020) Green synthesis of AgNPs() ultilizing *Delonix Regia* extract as anticancer and antimicrobial agents. Chem Select 5(42):13263–13268. https://doi.org/10.1002/slct.202003218

Adil SF, Assal ME, Khan M, Al-Warthan A, Siddiqui MRH, Liz-Marzán LM (2015) Biogenic synthesis of metallic nanoparticles and prospects toward green chemistry. Dalton Trans 44:9709–9717. https://doi.org/10.1039/C4DT03222E

Agressott EVH, Bläte D, Cunha FA, Noronha VT, Ciesielski R, Hartschuh A et al (2020) Vibrational Spectroscopy and morphological studies on protein capped biosynthesized silver nanoparticles. ACS Omega 5(1):386–393. https://doi.org/10.1021/acsomega.9b02867

Alves FS, Do Rego JAR, Da Costa ML, Da Silva LFL, Da Costa RA, Cruz JN, Brasil DSB (2020) Spectroscopic methods and in silico analyses using density functional theory to characterize and identify piperine alkaloid crystals isolated from pepper (Piper Nigrum L). J Biomol Struct Dyn 38(9):2792–2799. https://doi.org/10.1080/07391102.2019.1639547

Anandalakshmi K, Venugobal J (2017) Green synthesis and characterization of silver nanoparticles using *Vitex negundo* (Karu Nochchi) leaf extract and its antibacterial activity. Med Chem (los Angeles) 7:218–225. https://doi.org/10.4172/2161-0444.1000460

Anandalakshmi K, Venugobal J, Ramasamy V (2016) Characterization of silver nanoparticles by green synthesis method using *Pedalium murex* leaf extract and their antibacterial activity. Appl Nanosci 6:399–408. https://doi.org/10.1007/s13204-015-0449-z

Azmi SNH, Al-Jassasi BMH, Al-Sawafi HMS, Al-Shukaili SHG, Rahman N, Nasir M (2021) Optimization for synthesis of silver nanoparticles through response surface methodology using leaf extract of Boswellia sacra and its application in antimicrobial activity. Environ Monit Assess 93(8):498. https://doi.org/10.1007/s10661-021-09301-w

Biswas N, Kapoor S, Mahal HS, Mukherjee T (2007) Adsorption of CGA on colloidal silver particles: DFT and SERS study. Chem

Phys Lett 444:338–345. https://doi.org/10.1016/j.cplett.2007.07.049
Dresselhaus MS, Dresselhaus G, Saito R, Jorio A (2005) Raman spectroscopy of carbon nanotubes. Phys Rep 409(2):47–99. https://doi.org/10.1016/j.physrep.2004.10.006
Durán N, Marcato PD, Durán M, Yadav A, Gade A, Rai M (2011) Mechanistic aspects in the biogenic synthesis of extracellular metal nanoparticles by peptides, bacteria, fungi, and plants. Appl Microbiol Biotechnol 90(5):1609–1624. https://doi.org/10.1007/s00253-011-3249-8
Gorgani L, Mohammadi M, Najafpour GD, Nikzad M (2017) Piperine—the bioactive compound of black pepper: from isolation to medicinal formulations. Compr Rev Food Sci Food Saf 16:124–140. https://doi.org/10.1111/1541-4337.12246
Gour A, Jain NK (2019) Advances in green synthesis of nanoparticles. Artif Cells Nanomed Biotechnol 47:844–851. https://doi.org/10.1080/21691401.2019.1577878
Jacob SJP, Finub JS, Narayanan A (2012) Synthesis of silver nanoparticles using *Piper longum* leaf extracts and its cytotoxic activity against Hep-2 cell line. Colloids Surf, B 91:212–214. https://doi.org/10.1016/j.colsurfb.2011.11.001
Khan M, Khan M, Adil SF, Tahir MN, Tremel W, Alkhathlan HZ et al (2013) Green synthesis of silver nanoparticles mediated by *Pulicaria glutinosa* extract. Int J Nanomed 8(1):1507–1516. https://doi.org/10.2147/IJN.S43309
Kora AJ, Arunachalam J (2012) Green fabrication of silver nanoparticles by gum tragacanth (*Astragalus gummifer*): A dual functional reductant and stabilizer. J Nanomater. https://doi.org/10.1155/2012/869765
Lazarevska S, Geskovski N, Makreski P (2019) Deciphering the raman spectrum of royal jelly fabrication of Ag-polymer embedded royal jelly nanoparticles manifesting SERS effect. J Raman Spectrosc 50(12):1839–1848. https://doi.org/10.1002/jrs.5720
Li S, Li S-K, Gan R-Y, Song F-L, Kuang L, Li H-B (2013) Antioxidant capacities and total phenolic contents of infusions from 223 medicinal plants. Ind Crops Prod 51:289–298. https://doi.org/10.1016/j.indcrop.2013.09.017
Medjhouda Kebir ZA, Adel M, Adjdir M, Bengueddach A, Sassi M (2018) Preparation and antibacterial activity of silver nanoparticles intercalated kenyaite materials. Mater Res Express 5:085021. https://doi.org/10.1088/2053-1591/aacc7f
Mie R, Samsudin MW, Din LB, Ahmad A, Ibrahim N, Adnan SNA (2014) Synthesis of silver nanoparticles with antibacterial activity using the lichen *Parmotrema praesorediosum*. Int J Nanomed 9:121–127. https://doi.org/10.2147/IJN.S52306
Mollick MR, Rana D, Dash SK, Chattopadhyay S, Bhowmick B, Maity D, Mondal D, Pattanayak S, Roy S, Chakraborty M, Chattopadhyay D (2015) Studies on green synthesized silver nanoparticles using Abelmoschus esculentus (L.) pulp extract having anticancer (in vitro) and antimicrobial applications. Arab J Chem 12(8):2572–2584. https://doi.org/10.1016/j.arabjc.2015.04.033
Montes-García V, Pérez-Juste J, Pastoriza-Santos I, Liz-Marzán LM (2014) Metal nanoparticles and supramolecular macrocycles: a tale of synergy. Chem Eur J 20(35):10874–10883. https://doi.org/10.1002/chem.201403107
Mukherjee P, Roy M, Mandal BP, Dey GK, Mukherjee PK, Ghatak J, Tyagi AK, Kale SP (2008) Green synthesis of highly stabilized nanocrystalline silver particles by a non-pathogenic and agriculturally important fungus T asperellum. Nanotechnology 19:075103. https://doi.org/10.1088/0957-4484/19/7/075103
Obaid AY, Al-Thabaiti SA, El-Mossalamy EH, Al-Harbi LM, Khan Z (2017) Extracellular bio-synthesis of silver nanoparticles. Arab J Chem 10:226–231. https://doi.org/10.1016/j.arabjc.2014.12.035
Okitsu K, Yue A, Tanabe S, Matsumoto H, Yobiko Y (2001) Formulation of colloidal gold nanoparticles in an ultrasonic field: control of rate of gold (III) reduction and size of formed gold particles. Langmuir 17(25):7717–7720. https://doi.org/10.1021/la010414l
Paramelle D, Sadovoy A, Gorelik S, Free P, Hobley J, Fernig DG (2014) A rapid method to estimate the concentration of citrate capped silver nanoparticles from UV-visible light spectra. Analyst 139:4855–4861. https://doi.org/10.1039/C4AN00978A
Pelton JT, McLean LR (2000) Spectroscopic methods for analysis of protein secondary structure. Anal Biochem 277:167–176. https://doi.org/10.1006/abio.1999.4320
Rauf A, Ahmad T, Khan A, Uddin MG, Ahmad B, Mabkhot YN et al (2021) Green synthesis and biomedicinal applications of silver and gold nanoparticles functionalized with methanolic extract of *Mentha longifolia*. Artif Cells Nanomed Biotechnol 49(1):194–203. https://doi.org/10.1080/21691401.2021.1890099
Reddy NJ, Vali DN, Rani M, Rani SS (2014) Evaluation of antioxidant, antibacterial and cytotoxic effects of green synthesized silver nanoparticles by *Piper longum* fruit. Mater Sci Eng C 34:115–122. https://doi.org/10.1016/j.msec.2013.08.039
Rygula A, Majzner K, Marzec KM, Kaczor A, Pilarczyka M, Baranska M (2013) Raman spectroscopy of proteins: a review. J Raman Spectrosc 44:1061–1076. https://doi.org/10.1002/jrs.4335
Saddik MS, Elsayed MMA, Abdelkader MSA, Abdel-Aleem E-M, JA, Abu-Dief AM, Al-Hakkani MF, Farghaly HS, Abou-Taleb HA. (2021) Novel green biosynthesis of fluorouracil chromium nanoparticles using harpullia pendula extract for treatment of colorectal cancer. Pharmaceutics 13(2):226. https://doi.org/10.3390/pharmaceutics13020226
Sanpui P, Chattopadhyay A, Ghosh SS (2011) Induction of apoptosis in cancer cells at low silver nanoparticle concentrations using chitosan nanocarrier. Appl Mater Interfaces 3:218–228. https://doi.org/10.1021/am100840c
Sau TK, Pai A, Jana NR, Wang ZL, Pal T (2001) Size controlled synthesis of gold nanoparticles using photochemically prepared seed particles. J Nanopart Res 3:257–261. https://doi.org/10.1023/A:1017567225071
Schulz H, Baranska M, Quilitzsch R, Schütze W, Lösing G (2005) Characterization of peppercorn, pepper oil, and pepper oleoresin by vibrational spectroscopy methods. J Agric Food Chem 53:3358–3363. https://doi.org/10.1021/jf048137m
Shaik MR, Khan M, Kuniyil M, Al-Warthan A, Alkhathlan HZ, Siddiqui MRH, Shaik JP, Ahmed A, Mahmood A, Khan M, Adil SF (2018) Plant-Extract-Assisted Green Synthesis of Silver Nanoparticles Using *Origanum vulgare* L. Extract and Their Microbicidal Activities Sustainability 10(4):913. https://doi.org/10.3390/su10040913
Smilkov K, Gjorgieva Ackova D, Cvetkovski A, Ruskovska T, Vidovic B, Atalay M (2019) Piperine: old spice and new nutraceutical? Curr Pharm Des 25(15):1729–1739. https://doi.org/10.2174/1381612825666190701150803
Sun Y (2013) Controlled synthesis of colloidal silver nanoparticles in organic solutions: empirical rules for nucleation engineering. Chem Soc Rev 42:2497–2511. https://doi.org/10.1039/C2CS35289C
Zhang XF, Liu ZG, Shen W, Gurunathan S (2016) Silver nanoparticles: synthesis, characterization, properties, applications, and therapeutic approaches. Int J Mol Sci 17(9):1534. https://doi.org/10.3390/ijms17091534

Authors and Affiliations

Katarina Smilkov[1] · Darinka Gjorgieva Ackova[1] · Aleksandar Cvetkovski[1] · Nikola Geskovski[2] · Biljana Pejova[3] · Blazo Boev[4] · Petre Makreski[3]

Darinka Gjorgieva Ackova
darinka.gorgieva@ugd.edu.mk

Aleksandar Cvetkovski
aleksandar.cvetkovski@ugd.edu.mk

Nikola Geskovski
ngeskovski@ff.ukim.edu.mk

Biljana Pejova
biljana@pmf.ukim.mk

Blazo Boev
blazo.boev@ugd.edu.mk

Petre Makreski
petremak@pmf.ukim.mk

[1] Division of Pharmacy, Faculty of Medical Sciences, Goce Delčev University - Štip, Krste Misirkov No.10-A POB 201, 2000 Štip, Republic of North Macedonia

[2] Institute of Pharmaceutical Technology, Faculty of Pharmacy, Ss. Cyril and Methodius University in Skopje, Skopje, Republic of North Macedonia

[3] Institute of Chemistry, Faculty of Natural Sciences and Mathematics, Ss. Cyril and Methodius University in Skopje, Skopje, Republic of North Macedonia

[4] Faculty of Natural and Technical Sciences, Goce Delčev University - Štip, Štip, Republic of North Macedonia